

See discussions, stats, and author profiles for this publication at: <https://www.researchgate.net/publication/221809652>

# Ultrafast Intramolecular Exciton Splitting Dynamics in Isolated Low-Band-Gap Polymers and Their Implication in Photovoltaic Materials Design

ARTICLE *in* JOURNAL OF THE AMERICAN CHEMICAL SOCIETY · MARCH 2012

Impact Factor: 12.11 · DOI: 10.1021/ja209003y · Source: PubMed

---

CITATIONS

61

READS

28

## 6 AUTHORS, INCLUDING:



Jodi M Szarko

Northwestern University

43 PUBLICATIONS 1,397 CITATIONS

[SEE PROFILE](#)



Yongye Liang

South University of Science and Technology ...

67 PUBLICATIONS 14,049 CITATIONS

[SEE PROFILE](#)



Lin X. Chen

Northwestern University

416 PUBLICATIONS 8,283 CITATIONS

[SEE PROFILE](#)

# <sup>1</sup> Ultrafast Intramolecular Exciton Splitting Dynamics in Isolated Low-Band-Gap Polymers and Their Implications in Photovoltaic Materials Design

<sup>4</sup> Brian S. Rolczynski,<sup>†,‡,§</sup> Jodi M. Szarko,<sup>†,‡,§</sup> Hae Jung Son,<sup>‡,||</sup> Yongye Liang,<sup>||</sup> Luping Yu,<sup>\*,‡,||</sup> and Lin X. Chen<sup>\*,†,‡,§</sup>

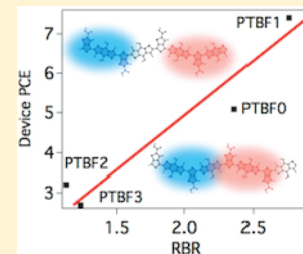
<sup>6</sup> <sup>†</sup>Department of Chemistry and <sup>‡</sup>ANSER Center, Northwestern University, 2145 Sheridan Road, Evanston, Illinois 60208, United States

<sup>8</sup> <sup>§</sup>Chemical Sciences and Engineering Division, Argonne National Laboratory, 9700 South Cass Avenue, Argonne, Illinois, 60439, United States

<sup>10</sup> <sup>||</sup>Department of Chemistry and The James Franck Institute, The University of Chicago, 929 East 57th Street, Chicago, Illinois 60637, United States

## <sup>12</sup> Supporting Information

**ABSTRACT:** Record-setting organic photovoltaic cells with PTB polymers have recently achieved ~8% power conversion efficiencies (PCE). A subset of these polymers, the PTBF series, has a common conjugated backbone with alternating thieno[3,4-*b*]thiophene and benzodithiophene moieties but differs by the number and position of pendant fluorine atoms attached to the backbone. These electron-withdrawing pendant fluorine atoms fine tune the energetics of the polymers and result in device PCE variations of 2–8%. Using near-IR, ultrafast optical transient absorption (TA) spectroscopy combined with steady-state electrochemical methods we were able to obtain TA signatures not only for the exciton and charge-separated states but also for an intramolecular (“pseudo”) charge-transfer state in isolated PTBF polymers in solution, in the absence of the acceptor phenyl-C<sub>61</sub>-butyric acid methyl ester (PCBM) molecules. This led to the discovery of branched pathways for intramolecular, ultrafast exciton splitting to populate (a) the charge-separated states or (b) the intramolecular charge-transfer states on the time scale of subpicoseconds to a few nanoseconds. Depending on the number and position of the fluorine pendant atoms, the charge-separation/transfer kinetics and their branching ratios vary according to the trend for the electron density distribution in favor of the local charge-separation direction. More importantly, a linear correlation is found between the branching ratio of intramolecular charge transfer and the charge separation of hole–electron pairs in isolated polymers versus the device fill factor and PCE. The origin of this correlation and its implications in materials design and device performance are discussed.



## 1. INTRODUCTION

Conjugated alternating copolymers, in which conjugated blocks with different electron affinities are alternately arranged in sequence along the polymer backbone, have recently shown relatively high power conversion efficiencies (PCEs) of >8% in bulk heterojunction (BHJ) organic photovoltaic (OPV) devices.<sup>1–3</sup> These higher PCEs, relative to those from benchmark homopolymers such as poly(3-hexylthiophene) (P3HT), are attributed in part to more efficient solar photon harvesting in the near-infrared (NIR) region due to a lower optical gap. Extensive studies on P3HT and its derivatives have rendered a wealth of information about the importance of the following factors upon device PCE: polymer regioregularity and conjugation length,<sup>4–6</sup> film morphology,<sup>7,8</sup> crystallinity,<sup>9</sup> molecular orientation,<sup>10,11</sup> charge carrier mobilities,<sup>12–14</sup> light harvesting efficiency in the solar spectrum,<sup>15</sup> and device fabrication conditions.<sup>16,17</sup> However, correlations between device performance and intrinsic properties of polymers, including structure, energetics, and charge carrier/exciton dynamics, remain unclear. In particular, the ultrafast exciton

splitting and charge carrier dynamics of the *isolated* donor polymers *in solution* have not been correlated directly to the device PCE because (a) a large number of parallel and sequential processes on both ultrafast and slow time scales occur only in device-relevant conditions and (b) only exciton splitting at the donor–acceptor BHJs is believed to determine the overall device PCE. It is commonly known that excitons split at donor–acceptor BHJs much faster and more efficiently than they do via intramolecular processes.<sup>18</sup> The LUMO energy level offset of the polymer and the PCBM has been used to estimate the driving force requirement for the exciton splitting,<sup>59</sup> but even this picture is inaccurate because it neglects the energy level modifications due to the BHJ. Since there is no apparent BHJ of isolated polymers in solution, there is no reason to expect that the polymer alone should have exciton dynamics relevant to the device. Therefore, optimization of donor polymers has been carried out largely upon the energetics via

Received: September 24, 2011

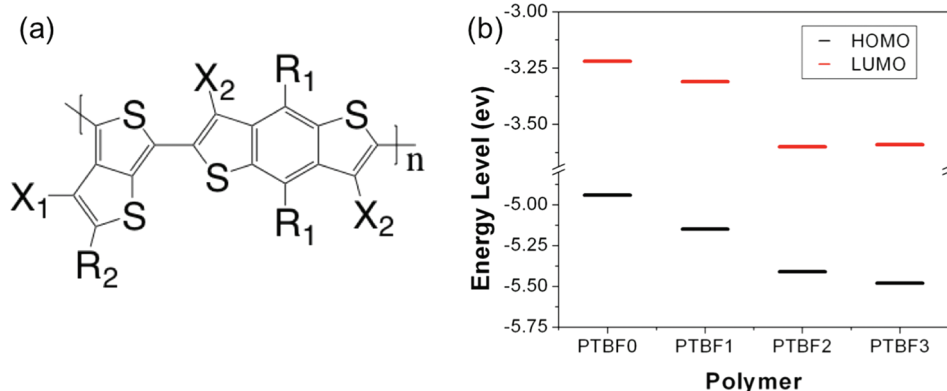


**Figure 1.** (a) PTBF series structure.  $R_1$  is oxyoctyl for PTBF0 and oxy(2-ethylhexyl) for PTBF1, PTBF2, and PTBF3.  $R_2$  is 2-ethylhexyl ester for all polymers.  $X_1$  is F for PTBF1 and PTBF2 and H otherwise.  $X_2$  is F for PTBF2 and PTBF3 and H otherwise. (b) HOMO and LUMO levels for the PTBF series as reported previously.<sup>17,26</sup>

tuning the ground and lowest singlet excited states of the polymer with respect to those of the electron acceptor, commonly phenyl-C<sub>61</sub>-butyric acid methyl ester (PCBM). For instance, recent research and development of OPV materials have yielded various new conjugated polymers<sup>18–23</sup> designed to (a) raise the PCE by achieving a higher open-circuit voltage ( $V_{OC}$ )<sup>24,25</sup> through lowering the polymer HOMO energy with respect to the LUMO of the PCBM and (b) extend the spectral overlap of the polymer absorption with the solar spectrum by decreasing the polymer's optical gap. Two closely related sets of these polymers have recently been synthesized, the PTB and PTBF series, which are composed of alternating, regioregular benzodithiophene (BDT) and thienothiophene (TT) moieties (Figure 1), where the electron affinity is higher in the TT.<sup>11,19</sup> The PTB series was originally developed by variation of the R and  $X_1$  positions, whereas the PTBF series was later developed by systematic fluorination at the  $X_1$  and  $X_2$  positions along the polymer fragment (Figure 1). The studies reported here are conducted on four polymers in the PTBF series, one of which was the first polymer to exhibit a high PCE (7.4%) in devices, while the PCE of the other polymers were 5.1%, 3.2%, and 2.7% for PTBF0, PTBF2, and PTBF3, respectively.<sup>1,18,26</sup>

Because the chemical structural differences in the PTBF series are minor, it is important to investigate what causes such significant variations in device PCE within this series of copolymers with similar molecular packing characteristics<sup>11</sup> and energetics.<sup>1,18,26</sup> This study highlights the importance of the intrinsic properties of alternating copolymers at a molecular level to the BHJ devices. In this report, we will demonstrate that these alternating copolymers in fact are not just p-type semiconductors acting as electron sources; they have intramolecular, ultrafast exciton splitting dynamics of their own and are capable of generating charge-transfer or charge-separated populations on a subpicosecond time scale. More interestingly, we observed that these polymers' intrinsic dynamic properties are closely correlated with device performance in BHJ films in the presence of the electron acceptor PCBM. This study searches for answers to the following questions: (a) how do the intramolecular exciton splitting dynamics depend on the moieties that make up the conjugated backbone, (b) what is the driving force for intramolecular charge separation, and (c) how are the intrinsic exciton splitting dynamics correlated with BHJ device parameters, such as fill factor (FF) and PCE?<sup>27</sup> Moreover, we will search for implications of these correlations

in materials design and OPV device optimization as well as long-term development of solar cell market viability.

## 2. EXPERIMENTAL AND COMPUTATIONAL METHODS

**2.1. Sample Preparation.** PTBF0, PTBF1, PTBF2, and PTBF3 (Figure 1) were synthesized according to a previously reported procedure.<sup>18,26</sup> Experimental details regarding the bulk device characteristics, such as  $I$ – $V$  curves,  $J_{sc}$ ,  $V_{oc}$ , FF, PCE, and polymer HOMO and LUMO energies, are also found in these sources. Solution samples were prepared in chlorobenzene (CB).

**2.2. Steady-State Absorption.** Steady-state absorption spectra (Figure 2) of solution and films were taken using a UV-3600 UV-vis-NIR spectrophotometer (Shimadzu, Columbia, MD).

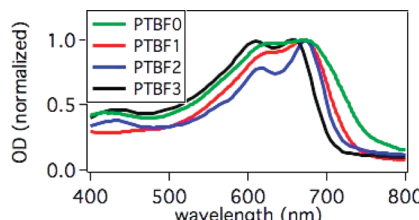


**Figure 2.** Normalized ground-state absorption spectra for the PTBF polymers.

To verify the polymer cation absorption features in solution, absorption spectra of the chemically oxidized polymer cation were measured in a spectral region of 200–1600 nm after titrating the solution samples with FeCl<sub>3</sub> (Aldrich). The chemically oxidized cation spectra were extracted by subtracting the spectra of the same solution prior to addition of FeCl<sub>3</sub> (see the Supporting Information).

**2.3. Electronic Structure Calculations.** Calculations were performed on model oligomers of corresponding PTBF polymers using the HyperChem software package (Hypercube, Inc., Gainesville, FL). Geometry optimizations of the oligomers with truncated aliphatic side chains were initiated using the AM1 parametrization. Calculations were subsequently carried out by the ZINDO/S method on both asymmetric (BDT-TT)<sub>4</sub> and symmetric TT-(BDT-TT)<sub>4</sub> tetramers. Configuration interaction (CI) calculations were performed using 20 orbitals above the HOMO and below the HOMO and LUMO gap.

**2.4. Transient Absorption Spectroscopy.** Transient absorption (TA) spectra were measured using an ultrafast laser system by Spectra-Physics at the Center for Nanoscale Materials in Argonne National Laboratory. A 600 nm pump beam at 1.67 kHz was generated by an optical parametric amplifier system (TOPAS, Light Conversion Ltd.) and pumped by a regenerative amplifier (Spitfire Pro, Spectra Physics Lasers) operating at a 5 kHz repetition rate. The Spitfire Pro was pumped by an Nd:YLF laser (Empower, Spectra-Physics Lasers) and

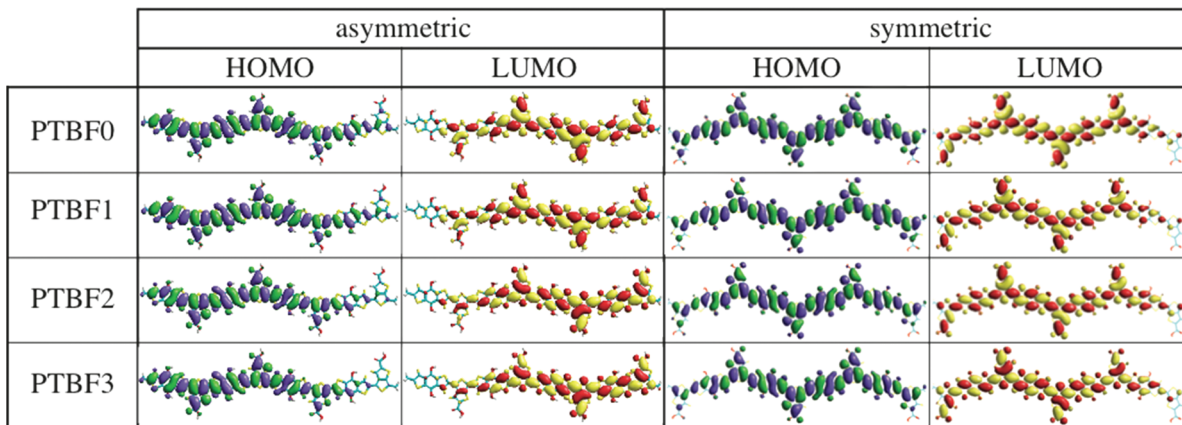


Figure 3. HOMO and LUMO for PTBF-like  $(BDT-TT)_4$  (left) and TT( $BDT-TT)_4$  (right) tetramers. Side chains are truncated for clarity.

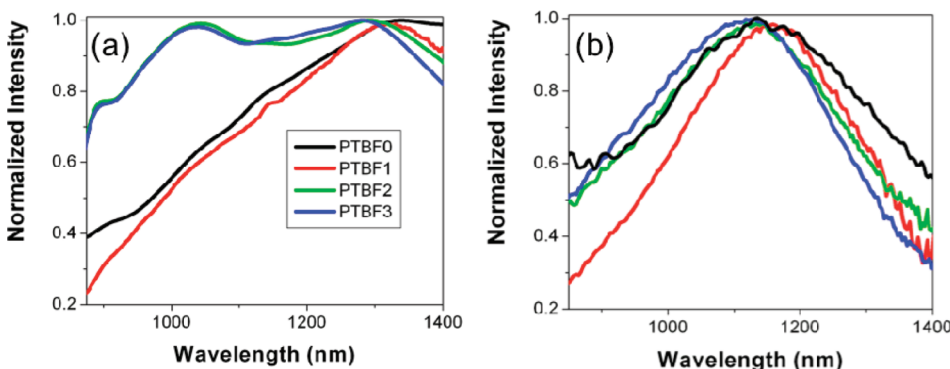


Figure 4. Normalized transient absorption spectra for the PTBF polymers at 2 ps (a) and 2.5 ns (b) pump–probe delay times. Excitation wavelength is 600 nm.

seeded by a Ti:sapphire oscillator (Tsunami, Spectra-Physics Lasers) that was pumped by a Nd:YVO<sub>4</sub> laser (Millennia, Spectra Physics Lasers). The output beam of the amplifier laser was split off and chopped at 833 Hz. These beams were used to pump a TA spectrometer (HELIOS, Ultrafast Systems LLC). A white light/NIR probe was generated by focusing the 800 nm beam into a sapphire plate. The 800–1500 nm component of this probe light was collected by a CCD device. The detection spectral region is 850–1400 nm. Samples were pumped at 600 nm using a focused 100  $\mu\text{m}$  diameter, 20 nJ/pulse. The cuvette path length was 2 mm, and the instrument response function (IRF) was 160 fs fwhm. NIR TA spectra were generated as two-dimensional data sets along time and wavelength axes.

### 3. RESULTS

**3.1. Calculated Electronic Structures.** PTBF0, PTBF1, PTBF2, and PTBF3 were modeled by their corresponding  $(BDT-TT)_4$  oligomers with energy-minimized structures using the AM1 method. The HOMO and LUMO for each species are shown in Figure 3. Calculations for the tetramers corresponding to PTBF0, PTBF1, PTBF2, and PTBF3 converged to binding energies of −270, −278, −285, and −292 MJ/mol, respectively, indicating a trend of lowering the energy via the number of pendant fluorines.

The CI calculations on model  $(BDT-TT)_4$  oligomers suggest that the lowest energy absorption band corresponds to mostly a HOMO–LUMO transition. The electron density distributions of HOMOs in these oligomers are more concentrated toward the BDT end, while those of LUMOs are more concentrated toward the TT end. Therefore, the HOMO–LUMO transition creates a net electron density shift from one segment of the

oligomer to the other segment, reminiscent of the charge separation in covalently linked donor–acceptor supermolecules in the literature.<sup>28</sup> When an additional TT unit is attached to  $(BDT-TT)_4$  to form a central symmetric TT( $BDT-TT)_4$  sequence (Figure 3), the HOMOs and LUMOs show a more evenly distributed electron density across the oligomers and the electron density shift due to the HOMO–LUMO transition is less pronounced compared to that in  $(BDT-TT)_4$  oligomers. The dipole moments of the corresponding BDT-TT monomer segments were also calculated and are shown in the Supporting Information.

### 3.2. Transient Absorption (TA) Spectra and Dynamics.

Normalized TA spectra of the PTBF polymers 2 ps after excitation by 600 nm light are shown in Figure 4a. These TA spectra are broad across the 900–1400 nm region but differ most strikingly near 1000 nm, where higher TA signals were found when the BDT moiety was fluorinated (PTBF2 and PTBF3). Kinetic traces taken in the 1350 nm region largely decay within 700–1000 ps, while those in the 950 nm region largely decay within 500–600 ps (Supporting Information). After these components decayed, a Gaussian-shaped feature at approximately 1150 nm remained. The normalized TA spectra of these polymers at 3 ns delay time (Figure 4b) show a single peak centered in the 1140–1160 nm region. Therefore, the time evolution of the TA spectra for the four polymers suggests the population of multiple states soon after excitation. Detailed analyses indicated that these TA spectra can be best approximated by three distinct Gaussian functions with their central positions at approximately 1000, 1150, and 1350 nm (see the Supporting Information).

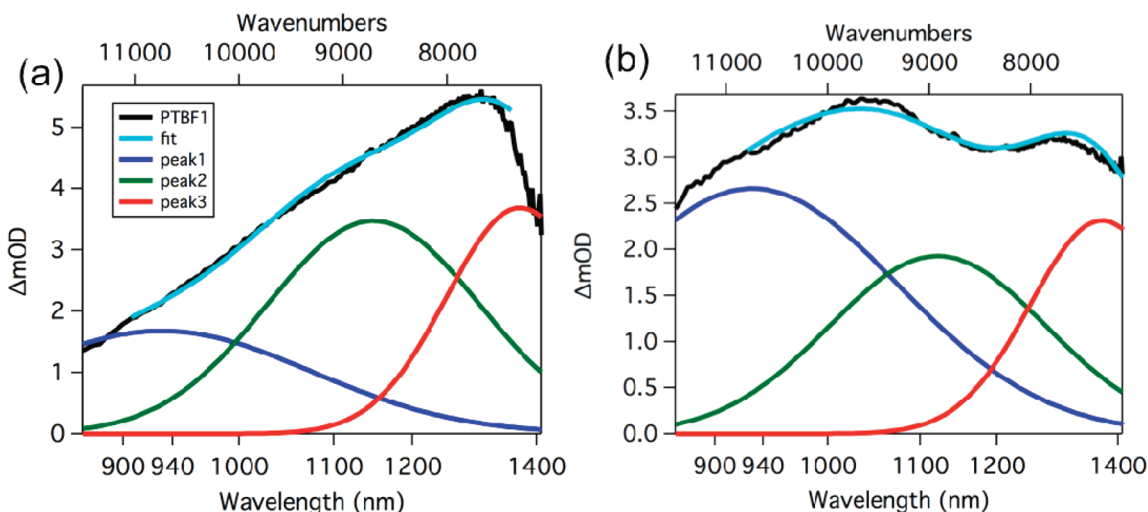


**Figure 5.** Transient absorption spectral fits of PTBF1 (a) and PTBF2 (b) at a delay time of 2 ps. This is an example of the spectral fit performed using a three-Gaussian fitting method (Supporting Information). Light blue curve is the sum of the three Gaussian curves representing the three spectral features identified in the spectrum, colored blue, green, and red.

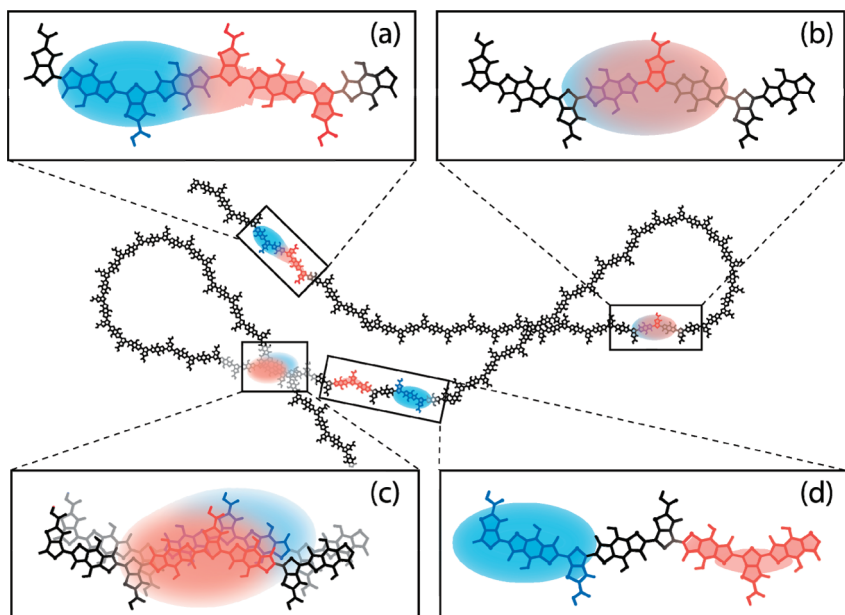


**Figure 6.** Illustration for delocalized electrons (red) and holes (blue) in intrachain PCT (a), EX (b), interchain PCT (c), and CS (d) states of an isolated polymer in solution.

The TA spectra of PTBF1 and PTBF2 are shown in Figure 5, along with the fits of the spectra using the three-component analysis (see the Supporting Information for details). The TA spectral feature at approximately 1150 nm is assigned to the polymer cation absorption. This assignment is based on two experimental observations. First, this signal coincides with the cation TA feature in the corresponding BHJ films with the same polymers and PCBM, where the charge separation is efficient and long lasting (the Supporting Information).<sup>10</sup> Second, this signal closely resembles the polymer cation features in the steady-state absorption spectrum after adding an oxidant  $\text{FeCl}_3$  into the solution (see the Supporting Information).

The broad TA feature around 1350 nm is assigned to the exciton (EX) state absorption for the following reasons. First, its lifetime agrees with other exciton lifetimes of 500–1000 ps in isolated polymers in the literature<sup>29</sup> and is much shorter than

the lifetime of the cation signal, which has a time constant of longer than a few nanoseconds. Second, it corresponds well to a TA feature in the same spectral region in the BHJ film (Figures S4 and S5 in the Supporting Information), whose decay corresponds well to the rise of the cation TA signal due to the EX-to-charge-separated (CS) state conversion. If the exciton-splitting process were slow, then the TA spectrum at early delay times would be almost entirely from the EX state as in previously studied conjugated homopolymers in solution<sup>29</sup> and the assignment would be straightforward. However, we observed evidence of subpicosecond generation of other states (to be described in detail later), so the earliest TA spectrum cannot be assigned solely to the EX state signal. The main interfering species at the early delay time is the cation, with its broad feature centered around 1150 nm, while the other feature around 1000 nm has much less influence on the EX signal. Hence, we subtracted a scaled TA spectrum at 3 ns delay from

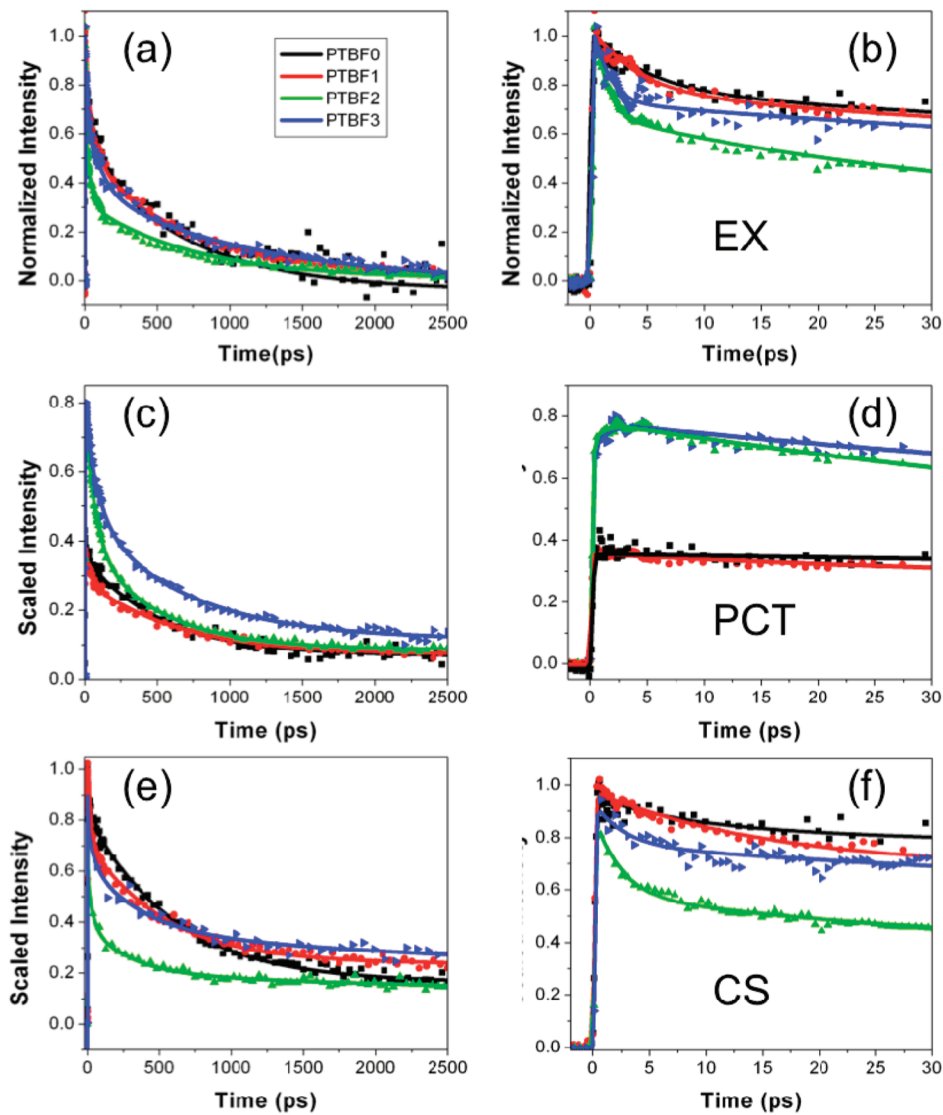


**Figure 7.** Kinetic traces for all transient spectroscopic features under investigation. Figures display 2500 (a, c, e) and 30 ps (b, d, f) of the kinetics. Fits are for EX (a, b), PCT (c, d), and CS (e, f) spectral features.

the initial TA spectrum, which resulted in a spectral feature at approximately 1350 nm that we assigned as the TA of the EX state. The scaling factor was based on the data analysis fits for the contributions from the other features, extrapolated to the early delay time based on kinetics parameters of other two TA features (see the Supporting Information).

In initial fits of the TA spectra with two Gaussian functions the reconstructed TA spectra did not fit well with the experimental data, as shown in the Supporting Information. Therefore, a three-Gaussian function fit was used, resulting in an almost perfect fit with very little residuals left in the difference spectra between the experimental spectra and the reconstructed TA spectra (Supporting Information). The three-Gaussian function fit of the TA data resulted in three broad peaks centered at approximately 1000, 1150, and 1350 nm. The additional feature at approximately 1000 nm is tentatively assigned to an intramolecular “pseudo”-charge-transfer (PCT) state. In this state, the exciton has split into a hole–electron pair that is still close enough to experience a Coulombic attraction.<sup>19,30</sup> Meanwhile, we also considered other possible assignments and subsequently ruled them out for the following

reasons. Triplet states can be ruled out because the formation (<1 ps) and decay (largely <1 ns) of this feature are both too short for conjugated polymers.<sup>29,31</sup> The polymer anion can be ruled out because the decay kinetics of this feature differ significantly from that of the cation. In addition, as will be discussed subsequently, this feature near 1000 nm also has a rise time correlating well with the decay of the EX peak in solution, indicating its generation is directly from the EX state. Also, blue shifting of the cation spectra has been reported in the literature due to counterion stabilization.<sup>32–37</sup> While there is no counterion in the TA experiment, the electron itself can act similarly to the counterion to stabilize the cation in an intramolecular charge-transfer state as long as it is proximal, which also fits the description of the PCT. Additionally, this transient species has precedence in other alternating copolymers in the literature.<sup>19,38</sup>

On the basis of the above considerations, the time-resolved 900–1400 nm TA spectra were fit to three Gaussian peaks at approximately 1000, 1150, and 1350 nm, whose intensities are used to characterize the kinetics of the three Gaussian spectral features, assigned to intramolecular pseudo-charge-transfer

**Table 1.** Time Constants ( $\tau$ ) and Pre-Exponential Weights (A) for EX, PCT, and CS State Transient Absorption Kinetics Fits<sup>a</sup>

sample	state	$\tau_1$ (ps)	$\tau_2$ (ps)	$\tau_3$ (ps)	$\tau_4$ (ps)	A <sub>1</sub> (%)	A <sub>2</sub> (%)	A <sub>3</sub> (%)	A <sub>4</sub> (%)
PTBF0	EX	5 (0.9)	99 (25)	700 (43)		23 (1.6)	23 (3.5)	54 (3.8)	
PTBF1	EX	4 (0.3)	87 (8)	800 (24)		25 (0.8)	27 (1.4)	47 (1.5)	
PTBF2	EX	1 (0.1)	31 (1)	730 (16)		40 (0.9)	30 (0.5)	30 (0.4)	
PTBF3	EX	1 (0.1)	100 (7)	1100 (41)		32 (1.3)	32 (1.3)	37 (1.3)	
PTBF0	PCT			525 (20)	>2800			87 (0.9)	13 (0.7)
PTBF1	PCT		40 (5)	632 (27)	>2800		19 (1.2)	60 (1.1)	21 (0.7)
PTBF2	PCT	1 (0.1)	71 (4)	480 (33)	>2800	(rise)	52 (2.4)	41 (2.3)	7 (0.2)
PTBF3	PCT	1 (0.1)	91 (10)	670 (68)	>2800	(rise)	41 (3.7)	50 (3.4)	9 (0.5)
PTBF0	CS	8 (1.1)		590 (14)	>2800	13 (0.6)		70 (0.5)	17 (0.6)
PTBF1	CS	14 (0.7)		518 (13)	>2800	26 (0.5)		50 (0.5)	25 (0.3)
PTBF2	CS	2 (0.1)	38 (2)	292 (4)	>2800	37 (1.3)	23 (0.4)	25 (0.3)	16 (0.1)
PTBF3	CS	3 (0.5)	53 (4)	377 (6)	>2800	19 (2.1)	17 (0.7)	35 (0.5)	29 (0.1)

<sup>a</sup>(Parentheses contain the standard deviation for each fitting parameter.

279 (PCT), charge-separated (CS), and exciton (EX) states (Figure  
280 6), respectively. The “pseudo” designation distinguishes this  
281 intramolecular charge-transfer state from donor:acceptor  
282 charge-transfer states that are more typically discussed in the  
283 literature. All three states have been characterized previously in  
284 other OPV materials by calculations<sup>39–41</sup> and experi-  
285 ments<sup>19,20,42</sup> in the literature.

286 Figure 7 displays kinetics scaled by the initial population of  
287 excitons extracted from global fits of the two-dimensional (time  
288 delay  $t$  and wavelength  $\lambda$ ) TA data sets,  $\Delta\text{OD}(t, \omega)$ . Each of  
289 these kinetics was subsequently fit to a Gaussian function in the  
290 energy dimension and multiplied to linear combinations of  
291 exponential functions in the delay time dimension with pre-  
292 exponential coefficients that reflect the time evolution for the  
293 populations of the three species at a particular wavelength. The  
294 two-dimensional TA data therefore can be expressed as  
295  $\Delta\text{OD}(\omega, t) = \sum_x B_x(\omega) \sum_n A_n^x(\omega) \exp(-t/\tau_n^x)$ , where  $x$  denotes  
296 EX, PCT, or CS,  $n$  is the index of the exponential components,  
297  $\tau$  is the time constant,  $t$  is the time delay between the pump and  
298 probe pulses, and  $A_n^x(\omega)$  is the weight of the  $n$ th exponential  
299 component of transient species  $x$  at the probe energy expressed  
300 in wavenumber  $\omega$ . The fitting parameters and their standard  
301 deviations are shown in Table 1, and the parameters for  $B(\omega)$   
302 are shown in Table S1 in the Supporting Information.

303 The EX kinetics (Figure 7a and 7b) of all polymers are best  
304 fit by a sum of three exponential components,  $n = 1–3$  (Table  
305 1). The EX-to-PCT and EX-to-CS conversions largely occur  
306 within the 160 fs instrument response function time, similar to  
307 what was predicted theoretically for a different isolated  
308 conjugated polymer, polyphenylenevinylene (PPV).<sup>41</sup> The  
309 long decay time constant,  $\tau_3^{\text{EX}} = 700–1100$  ps, is similar to  
310 the exciton lifetime in isolated P3HT.<sup>29,43</sup> Hence,  $\tau_3^{\text{EX}}$  in the  
311 EX kinetics most likely arises from the excitons that do not  
312 undergo the EX-to-PCT or EX-to-CS processes.

313 The PCT spectral feature (Figure 7c and 7d) is generated  
314 within the IRF time in all polymers. However, only PTBF2 and  
315 PTBF3 have an additional rise of this feature with a time  
316 constant of  $\tau_1^{\text{PCT}} = 1$  ps, which correlated well with a  
317 concurrent decay component of the EX signal but not with the  
318 ground-state bleach (GSB) signal (Figure S7, the Supporting  
319 Information). Hence, this kinetic process is most likely due to  
320 an additional slower PCT generation process after the  
321 instantaneous process unresolved in our TA setup with a 160  
322 fs IRF (see the Supporting Information). The rise of the PCT  
323 population in PTBF2 and PTBF3 is ascribed to intramolecular,  
324 geminate hole–electron pair trapping after localized exciton

splitting, which generates the initial EX-to-PCT and EX-to-CS conversion in <160 fs in PTBF0 and PTBF1 (Figure 8).

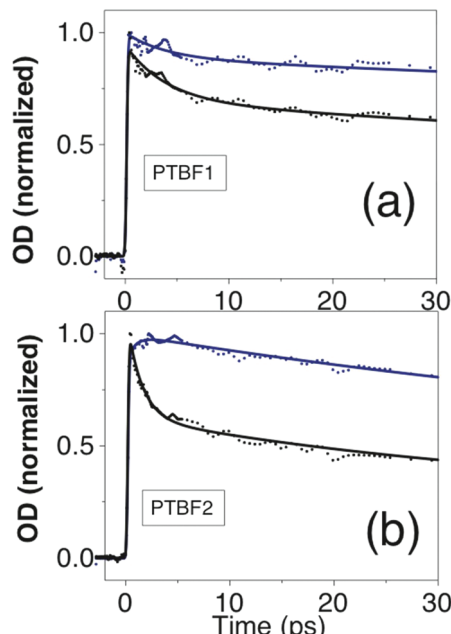


**Figure 8.** Transient absorption EX (black) and PCT (blue) kinetics for PTBF1 (a) and PTBF2 (b). PTBF2 exhibits a concurrent decay in the EX population and rise in the PCT population, while the PTBF1 population does not.

Intramolecular exciton splitting occurs on a time scale much smaller than 100 fs, as calculated by Bedard-Hearn et al.<sup>41</sup> Therefore,  $\tau_1^{\text{PCT}}$  is too long to account for ultrafast exciton delocalization generally on the time scale of ~100 fs.<sup>41</sup> Due to their lifetimes,<sup>19</sup> the two other decay time constants of the PCT feature,  $\tau_2^{\text{PCT}}$  and  $\tau_3^{\text{PCT}}$ , are assigned, respectively, to intrachain geminate recombination and interchain recombination of charge carriers occurring across self-aggregated polymer fragments of a single polymer (Figure 6).

The CS kinetics (Figure 7e and 7f) were obtained by the spectral signal of the polymer cation. As opposed to BHJ film kinetics, the entire cation population in isolated polymers in solution is generated within 160 fs after photoexcitation. Subsequently, the shortest decay time constant  $\tau_1^{\text{CS}}$  is 2–3 ps for PTBF2 and PTBF3 and 8–13 ps for PTBF0 and PTBF1. PTBF2 and PTBF3 also exhibit an additional decay channel

343  $\tau_2^{\text{CS}}$  at 21 (24%) and 98 ps (23%), respectively. The time  
 344 constant  $\tau_3^{\text{CS}}$  is 270–650 ps and has a larger pre-exponential  
 345 weight as the number of fluorine atoms decreases.

#### 4. DISCUSSION

346 **4.1. Influence of Polymer Local Electronic Structures**  
 347 **on Exciton and Charge-Separation Dynamics.** One major  
 348 consideration for achieving a high PCE in OPV devices is  
 349 overcoming the exciton binding energy in order to achieve  
 350 efficient charge separation.<sup>44</sup> This challenge is typically  
 351 addressed using a BHJ architecture and relying on the  
 352 LUMO energy offset between the donor polymer and the  
 353 acceptor (e.g., PCBM) at their interface to split the  
 354 exciton.<sup>26,45,46</sup> This LUMO energy offset requirement of  
 355 ~0.3–0.5 eV approximates the exciton splitting driving force  
 356 based on the Marcus–Hush model<sup>47</sup> and assumes that the  
 357 lowest energy electronic transition is almost entirely a  
 358 HOMO–LUMO transition of the donor polymer.<sup>48</sup> However,  
 359 this current picture ignores structural details at the donor–  
 360 acceptor interfaces as well as the local field effects by charged  
 361 species which could significantly alter the redox potentials and  
 362 energies of relevant states.<sup>23</sup> Moreover, alternating copolymers  
 363 deviate from the trend between charge-separation driving force  
 364 and geminate recombination efficiency, which has been found  
 365 for several homopolymer OPV materials (e.g., P3HT).<sup>23,49</sup> For  
 366 example, some alternating copolymers exhibit a lower driving  
 367 force of 0.1–0.2 eV required for achieving low geminate  
 368 recombination and high cation populations, such as  
 369 PCPDTBT.<sup>21</sup> These exceptions suggest the importance of  
 370 intramolecular local structural details in estimating energetic  
 371 costs for exciton splitting in alternating copolymers, such as the  
 372 relative distance and orientation of the donor and acceptor at  
 373 the domain interface in the BHJ films as well as the intrinsic  
 374 electronic structures of the alternating blocks along the polymer  
 375 chain.

376 As discussed earlier, the electron affinity of TT is higher than  
 377 that of BDT in the PTBF polymer series, which establishes a  
 378 local electron density gradient along the polymer backbone.  
 379 Additional electron-withdrawing fluorine atoms will further  
 380 modulate the electron density distribution in the ground and  
 381 excited states. For example, adding a fluorine atom at the X<sub>1</sub>  
 382 position on TT to form **PTBF1** (Figure 1) will enhance the  
 383 electron-pulling effect toward TT, resulting in higher local  
 384 charge-transfer character. In comparison, adding fluorine atoms  
 385 at two X<sub>2</sub> positions in **BDT** instead at the X<sub>1</sub> position to form  
 386 **PTBF2** will pull the electron density in an opposite direction,  
 387 away from TT, and partially negate the electron-withdrawing  
 388 direction established in **PTBF1**. Furthermore, adding three  
 389 fluorine atoms at X<sub>1</sub> and X<sub>2</sub> to form **PTBF3** will again pull the  
 390 electron slightly toward TT compared to that in **PTBF2**. These  
 391 “push–pull” actions on the electron density are reflected in the  
 392 magnitudes of local electronic dipole moments in the  
 393 monomers of all four polymers in an order of **PTBF1** >  
 394 **PTBF0** > **PTBF3** > **PTBF2** (Supporting Information) and  
 395 cause subtle yet important differences in the intramolecular  
 396 exciton splitting dynamics and relative populations of the  
 397 transient species in the PTBF as well as other polymers.<sup>26,50</sup> As  
 398 shown in previous work,<sup>1,26</sup> such chemical modifications also  
 399 influence the device performance significantly. Here, we intend  
 400 to rationalize the effects by differences in the local electronic  
 401 structures of the polymer chain and their implications for  
 402 device performance.

Our studies have revealed that isolated **PTBF** polymers *alone*  
 403 are capable of intramolecular charge transfer between adjacent  
 404 polymer moieties, but their exciton dynamics and initial relative  
 405 populations of EX, PCT, and CS states vary. In order to  
 406 understand these results, we first need to know what the  
 407 equivalent electron donor and acceptor are in isolated  
 408 copolymers and what drives intramolecular charge separation  
 409 in the absence of external electron acceptor.  
 410

In isolated conjugated homopolymers such as P3HT, exciton  
 411 splitting originates from the localization of an initially  
 412 delocalized exciton to form a polaron, driven by nuclear  
 413 reorganization upon a shift in charge density, and consequent  
 414 formation of a Coulombically bound, closely located electron–  
 415 hole pair.<sup>51</sup> This suggests that exciton splitting is facilitated by a  
 416 local asymmetry of electron density or charge gradients in  
 417 combination with the structural reorganization that results in a  
 418 potential energy barrier to prevent geminate recombination.  
 419 Because of the built in local electron density gradient along the  
 420 polymer backbone, the initial exciton splitting mechanism will  
 421 be significantly different in alternating copolymers. Compre-  
 422 hensive calculations by Risko, McGehee, and Brédas on the  
 423 electronic structures of several oligomer models corresponding  
 424 to alternating copolymers showed that the first excited state S<sub>1</sub>  
 425 was dominated by the HOMO–LUMO transition (>90%),  
 426 accompanied by significant electron density displacement along  
 427 the polymer backbone.<sup>52</sup> Such an electron density displacement  
 428 in the exciton was also seen in our calculations in the model  
 429 tetramers (Figure 3), implying that a “hole”-like electron  
 430 density depletion is produced in one segment while an  
 431 “electron”-like electron density enrichment is simultaneously  
 432 generated in another segment of the polymer, resulting in a  
 433 polarized exciton.  
 434

Because isolated polymer chains in solution are known to  
 435 have C–C bond twists, resulting in  $\pi$ -conjugation disruptions  
 436 and local structural variations or defects, it is difficult to identify  
 437 accurately the electron donor and acceptor segments in these  
 438 isolated polymers as shown in Figures 3 and 6. Moreover, the  
 439 size of the exciton, a range of the effective displacement of the  
 440 electron density from HOMO to LUMO, is unclear from  
 441 calculations with a limited length of the backbone. Although  
 442 large-scale computations combining molecular dynamics  
 443 simulation with quantum mechanical theory may verify this  
 444 proposed intramolecular electron donor–acceptor model, such  
 445 calculations are beyond the scope of the current work.  
 446 Nevertheless, the calculated results of HOMO–LUMO  
 447 electron density distributions (**BDT**–TT)<sub>4</sub> and TT–(**BDT**–  
 448 TT)<sub>4</sub> oligomers (Figure 3) provide a basis for a segmented  
 449 donor and acceptor model due to the electron gradient across  
 450 the polymer chain.  
 451

The above model suggests a possible general mechanism for  
 452 intramolecular charge separation in the alternating polymers,  
 453 while different exciton-splitting dynamic behaviors among the  
 454 four **PTBF** polymers need to be further explained in terms of  
 455 fine tuning the electronic structures by the pendant fluorine  
 456 atoms. The order of magnitude of the dipole moment change  
 457  $\Delta\mu_{\text{eg}}$  (i.e.,  $\mu_{\text{ex}} - \mu_{\text{gs}}$ ) in monomers via a HOMO–LUMO  
 458 transition suggests that **PTBF1** could potentially have the most  
 459 polarized exciton, with the largest effective electron–hole  
 460 displacement compared to the excitons of other polymers in  
 461 this series. Consequently, **PTBF1** has the highest relative CS/  
 462 PCT population as well as the highest PCE from our previous  
 463 studies.<sup>26</sup> In contrast, **PTBF2** has the smallest  $\Delta\mu_{\text{eg}}$  upon the  
 464 HOMO–LUMO transition and the highest initial PCT  
 465

466 population, which lead to geminate recombination of the hole  
 467 and electron. Evidently, a larger local  $\Delta\mu_{eg}$  facilitates a better  
 468 hole–electron separation in the exciton state, implying this  
 469 more polarized exciton makes charge separation easier. In  
 470 contrast, the smallest dipole change in the monomer of PTBF2  
 471 is due to the electron density being pulled in opposite  
 472 directions by two electron-withdrawing sources, fluorine atoms  
 473 on TT and BDT units. Apparently, for exciton splitting in  
 474 conjugated polymers, a larger local dipole change is desirable,  
 475 which can be rationalized by a larger resulting hole and electron  
 476 distance to weaken the attractive Coulombic interactions.

477 Besides the intrinsic local dipole moment change in these  
 478 polymers, the energy difference between the EX and the CS or  
 479 PCT states needs to be considered in the EX-to-PCT and EX-  
 480 to-CS processes. As an exciton splits, the resulting hole–  
 481 electron separation could initially have different separation  
 482 distances according to the excess energy and local environment.  
 483 A larger  $\Delta\mu_{eg}$  facilitates the EX-to-CS process with resulting  
 484 large hole–electron separation distances, while a smaller  $\Delta\mu_{eg}$   
 485 stabilizes strongly interacting hole–electron pairs in the PCT  
 486 state at a lower energy than the CS state (Figure 9). PTBF2

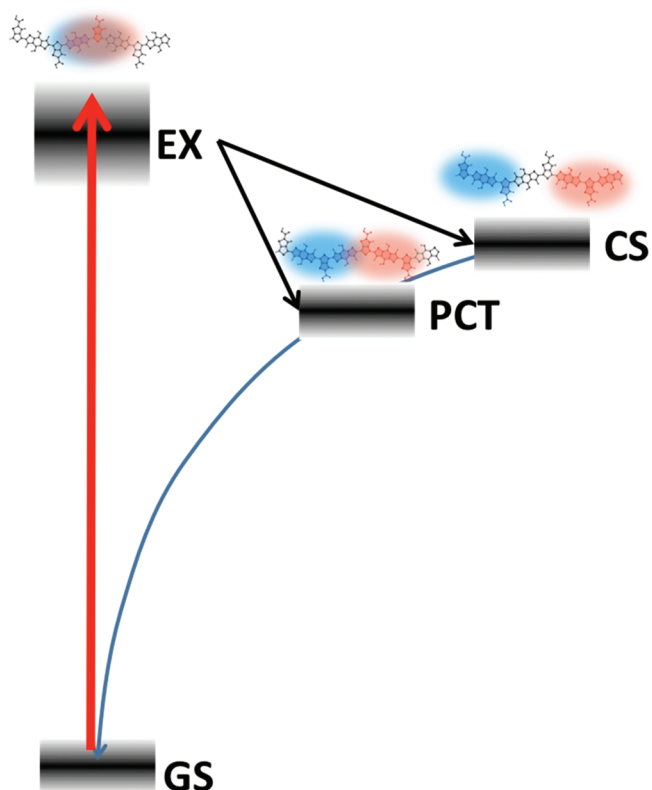


Figure 9. Schematic illustration of the states and pathways involved in the early exciton splitting dynamics of the isolated PTBF polymers in solution. Fuzzy energy levels describe the energy dispersion due to the structural inhomogeneity in isolated polymers in solution. Holes are indicated with a blue region on the polymer backbone, while electrons are indicated in red. Size of these regions provides a qualitative description of the hole and electron delocalization only. Curved downward arrow follows the potential energy as a function of the hole–electron separation as approximated in the Onsager model as well as the direction of the recombination for the CS and PCT states. GS denotes the ground state.

487 and PTBF3 polymers with smaller monomer  $\Delta\mu_{eg}$  not only  
 488 have the higher PCT population within the IRF time but also

489 show additional formation of PCT for the EX-to-PCT 489 conversion during EX localization. In contrast, PTBF0 and 490 PTBF1, with larger  $\Delta\mu_{eg}$  values in the polymer fragments, favor 491 EX-to-CS conversion processes and are only able to undergo 492 the EX-to-PCT transition in <160 fs, when the excitons may 493 not yet have been as strongly confined by nuclear motions.<sup>51</sup> In 494 both cases, the “push–pull” character in these polymers has 495 defrayed a part of the cost for exciton splitting to produce the 496 CS and PCT states. If an external acceptor is in the proximity to 497 the electron density-rich segment in the backbone, forming a 498 “donor–acceptor1–acceptor2 triad”, it can take the electron 499 that has already been intramolecularly separated from the hole, 500 reducing the required exciton splitting driving force. 501

#### 4.2. Branched Pathways from Exciton to Charge 502

Separation. A simplified energy diagram with dynamic 503 pathways is proposed for intramolecular processes (Figure 9). 504 Local conformational variation in the polymers results in 505 energy variation of the three states; hence, the TA features of 506 these states are inhomogeneously broadened. The PCT state 507 has a lower potential energy than the CS state because the 508 separated, yet closely positioned, hole–electron pairs experi- 509 ence an attractive Coulombic interaction that stabilizes the 510 PCT state.<sup>23</sup> Different polarities due to the intrinsic dipole 511 change of the polymer or the surroundings will affect the local 512 dielectric constant and exciton polarization and hence the initial 513 hole–electron separation distance. 514

This model agrees with our experimental observation, where 515 the EX-to-PCT conversion is prominent in PTBF2 and PTBF3 516 while the EX-to-CS process dominates in PTBF1 and PTBF0. 517 Because the PCT state on average has shorter hole–electron 518 separation, the former two polymers are more in favor of 519 trapping for the strongly bound electron–hole pair originated 520 from intramolecular exciton splitting. In reality, the trans- 521 formation from EX to PCT and CS could coexist depending on 522 local structure. Here, we suggested branched pathways of EX- 523 to-CS and EX-to-PCT that could coexist and the different 524 PTBF polymers (Figure 9), according to their electronic 525 structures and polarity of the exciton, could have their 526 preferences. 527

#### 4.3. Influence of the Branched Exciton Pathways on 528

Device Performances. To determine the importance of 529 branching ratio for intrachain exciton splitting from EX to PCT 530 or CS, we defined a parameter named the *relative* branching 531 ratio (RBR) that is the ratio of the two amplitude coefficients 532  $A_{CS}/A_{PCT}$  at the time after photoexcitation when the PCT 533 signal is maximized. Note that the RBR does not give an exact 534 ratio of the CS and PCT populations because the extinction 535 coefficients for these states are not necessarily equal, while the 536 extinction coefficients for the same species are assumed to be 537 the same across the four polymers. To our surprise, linear 538 correlations between the RBR of the isolated polymer *in* 539 *solution* and the PCE and FF of the BHJ *devices* made from 540 these polymers<sup>26</sup> appear with good fidelity ( $r^2 = 0.91$  or 0.97, 541 respectively) (Figure 10), even though potentially important 542 factors for the BHJ performance (e.g., polymer packing or 543 donor:acceptor potential energy offsets) are absent. However, 544 only a poor correlation of RBR and device  $V_{oc}$  was observed in 545 the PTBF polymer series.<sup>24,25</sup> While the cause of such 546 correlations is not fully understood, such intramolecular RBR 547 and BHJ device PCE connections have not been observed 548 previously. This correlation emphasizes that a molecular 549 picture, with a focus on local intramolecular interactions 550 instead of the commonly used energy band model, is more 551

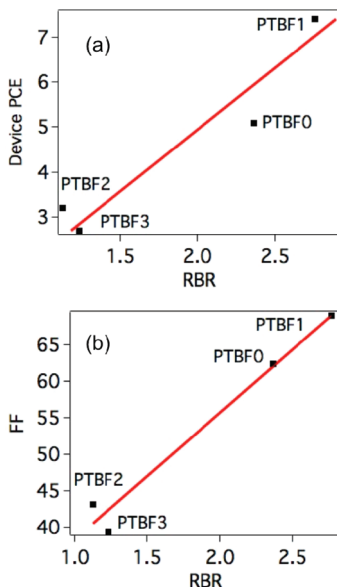


**Figure 10.** Relative branching ratios (RBR) of CS/PCT populations for polymer solutions versus OPV device PCE (a) and FF (b).

important than we previously thought in OPV applications using these low-band-gap polymers with charge-transfer character. This observation therefore carries implications in future OPV polymer design, where not only the position of the donor and acceptor energy levels but also the local structure facilitates that splitting excitons needs to be considered.

A linear relationship between solution RBR and device PCE or FF also implies that CS and PCT states in isolated charge-transfer copolymers could be precursors for or closely related to the CS and trapped CT states in the BHJ films. Because most of the intramolecular EX-to-CS and EX-to-PCT processes occur in <160 fs in these polymers, the relative populations of CS and PCT have been established before the intermolecular charge transfer to PCBM in BHJs.<sup>10</sup> Therefore, the CS state population is proportional to the free charge carrier populations, while the trapped PCT state population leads to the geminate recombination. When the intramolecular CS takes place, it preseparates hole and electron pairs and hence defrays a part of the cost for charge separation between the donor copolymer and PCBM. This makes it less energetically expensive for an acceptor to subsequently extract the electron, because that acceptor no longer pays the full cost of counteracting the Coulombic hole–electron attraction of an exciton. Hence, the polymer's intramolecular CS state population is energetically favorable for external electron acceptors to extract electrons from the polymer due to its relatively weak Coulombic attraction between electrons and holes. In comparison, the energetic cost for an external electron acceptor to extract an electron from the polymer's PCT state is higher due to a stronger Coulombic attraction between the hole–electron pair. On the basis of the a good correlation between RBR and FF in this series, fine tuning the “push–pull” interaction between neighboring monomers such that the CS/PCT population ratio is maximized is a promising method to optimize PCE and FF and potentially could be performed simultaneously to  $V_{oc}$  optimization. Our results also point out that an increase in the exciton polarity would enhance the CS state population and even the device PCE or FF, but this

hypothesis will be further investigated through new materials in our future studies.

**4.4. Implications of the “Defrayed Energetic Cost” in OPV Polymer Design.** As new and more complex polymers are synthesized for OPV applications, the contemporary organic semiconductor picture for conjugated polymers needs to be revised for the alternating “push–pull” copolymers where localized, ultrafast, molecule-like behaviors could play important roles in the OPV functions and even in photovoltaic devices. In the process of improving the device PCE through chemical tuning one needs to consider a balance between factors which may not be fully appreciated. This balance is between harnessing the optimal driving force to generate free carriers from excitons and generating Coulombically trapped charge carriers that are more difficult for the acceptor to extract. The former would lead to more efficient charge extraction in an OPV device, while the latter would lead to less. Therefore, the intramolecular PCT kinetics discussed here suggest a need to rethink charge pair trapping and exciton splitting for alternating copolymers based on the electronegativity and position of the backbone's pendant moieties, because these events are usually considered to be intermolecular, occurring at the donor:- acceptor boundary of BHJs, but our results show that actually the intramolecular processes are also significant. Designing polymers that induce these events in an optimal ratio may lead to improved device efficiency, especially if future polymers can be tuned to preferentially generate CS population intramolecularly. Further research must be done to understand the losses associated with inducing these intramolecular charge traps and driving forces, the extent to which they can be optimized.

## 5. CONCLUSION

We addressed the significance of intramolecular pseudo-charge transfer (PCT) and charge-separated (CS) states in four polymers of the PTBF species in solution. Our studies indicate that polymer modifications by fluorination tune the energy levels of the polymers with respect to the intramolecular PCT and CS states, which leads to a delicate balance in populating the CS or PCT states and to two possible outcomes in the intramolecular transient population, desirable charge separation or undesirable charge trapping. Finally, the dependence of these states on solar device efficiency was also highlighted. These findings suggest a systematic method to modulate the extent of intramolecular charge separation or pseudo-charge transfer in alternating copolymers, and their surprisingly well-correlated relationship to device performance has been brought to the OPV community's attention in designing alternating “donor–acceptor” copolymer systems. Our study reveals the origin of such a connection and suggests that these copolymers distinctly differ from previously studied homopolymers because of their local molecule-like nature that may play important roles in device performance. The intramolecular exciton separation driving force suggests the presence of a charge-separating “triad” by two hole-rich and electron-rich segments along the polymer backbone with the external electron acceptor PCBM at the BHJs, to facilitate charge transfer with less geminate recombination, as well as to hinder the geminate recombination. The details of these two outcomes in BHJ films, the nature of the RBR and device parameter correlations, will be discussed in our future reports.

## 649 ■ ASSOCIATED CONTENT

## 650 ■ Supporting Information

651 Discussion of sample conditions, fitting protocol for transient  
 652 absorption data, ground-state bleach comparison, conditions for  
 653 reduction of exciton–exciton annihilation signal, oxidized  
 654 polymer steady-state absorption, and dipole monomer  
 655 calculations. This material is available free of charge via the  
 656 Internet at <http://pubs.acs.org>.

## 657 ■ AUTHOR INFORMATION

## 658 Corresponding Author

659 E-mail: lchen@anl.gov; lupingu@uchicago.edu

## 660 Notes

661 The authors declare no competing financial interest.

## 662 ■ ACKNOWLEDGMENTS

663 This research was supported by the ANSER Center, an Energy  
 664 Frontier Research Center funded by the U.S. Department of  
 665 Energy, Office of Science, Office of Basic Energy Sciences,  
 666 under Award Number DE-SC0001059. Part of the equipment  
 667 and laboratory setting was supported by the Division of  
 668 Chemical Sciences, Office of Basic Energy Sciences, the U.S.  
 669 Department of Energy under contract DE-AC02-06CH11357  
 670 (for L.X.C.). The gift from Intel Corp. to L.X.C. and L.Y. is  
 671 greatly appreciated for a part of research related to film  
 672 fabrication. We also thank Drs. David J. Gosztola and Gary  
 673 Wiederrecht for their help in the Center for Nanoscale  
 674 Materials at Argonne National Laboratory. Use of the facilities  
 675 at the Center for Nanoscale Materials was supported by the  
 676 U.S. Department of Energy, Office of Science, Office of Basic  
 677 Energy Sciences, under Contract No. DE-AC02-06CH11357.

## 678 ■ REFERENCES

- 679 (1) Liang, Y.; Xu, Z.; Xia, J.; Tsai, S.-T.; Wu, Y.; Li, G.; Ray, C.; Yu, L. *Adv. Mater.* **2010**, *22*, E135.
- 680 (2) He, Z.; Zhong, C.; Huang, X.; Wong, W.-Y.; Wu, H.; Chen, L.; Su, S.; Cao, Y. *Adv. Mater.* **2011**, *23*, 4636.
- 681 (3) Chen, H.-Y.; Hou, J.; Zhang, S.; Liang, Y.; Yang, G.; Yang, Y.; Yu, L.; Wu, Y.; Li, G. *Nat. Photonics* **2009**, *3*, 649.
- 682 (4) Korovyanko, O. J.; Österbacka, R.; Jiang, X. M.; Vardeny, Z. V.; Janssen, R. A. *J. Phys. Rev. B* **2001**, *64*, 235122.
- 683 (5) Szarko, J. M.; Rolczynski, B. S.; Guo, J.; Liang, Y.; He, F.; Mara, M. W.; Yu, L.; Chen, L. X. *J. Phys. Chem. B* **2010**, *114*, 14505.
- 684 (6) Schwartz, B. *J. Annu. Rev. Phys. Chem.* **2003**, *54*, 141.
- 685 (7) Pingree, L. S. C.; Reid, O. G.; Ginger, D. S. *Adv. Mater.* **2009**, *21*, 691.
- 686 (8) Rance, W. L.; Ferguson, A. J.; McCarthy-Ward, T.; Heeney, M.; Ginley, D. S.; Olson, D. C.; Rumbles, G.; Kopidakis, N. *Ac Nano* **2011**, *5*, 5635.
- 687 (9) Joshi, S.; Grigorian, S.; Pietsch, U. *Phys. Status Solidi A* **2008**, *205*, 696.
- 688 (10) Guo, J.; Liang, Y.; Szarko, J.; Lee, B.; Son, H. J.; Rolczynski, B. S.; Yu, L.; Chen, L. X. *J. Phys. Chem. B* **2010**, *114*, 742.
- 689 (11) Szarko, J. M.; Guo, J.; Liang, Y.; Lee, B.; Rolczynski, B. S.; Strzalka, J.; Xu, T.; Loser, S.; Marks, T. J.; Yu, L.; Chen, L. X. *Adv. Mater.* **2010**, *22*, 5468.
- 690 (12) Sirringhaus, H.; Brown, P. J.; Friend, R. H.; Nielson, M. M.; Bechgaard, K.; Langeveld-Voss, B. M. W.; Spiering, A. J. H.; Janssen, R. A. J.; Meijer, E. W.; Herwig, P.; Leeuw, D. M. d. *Nature* **1999**, *401*, 705.
- 691 (13) Dante, M.; Peet, J.; Nguyen, T. *J. Phys. Chem. C* **2008**, *112*, 707.
- 692 (14) Coffey, D. C.; Ferguson, A. J.; Kopidakis, N.; Rumbles, G. *ACS Nano* **2010**, *4*, 5437.
- 693 (15) Lewis, N. S. *Science* **2007**, *315*, 798.
- 694 (16) Ma, W.; Yang, C.; Gong, X.; Lee, K.; Heeger, A. J. *Adv. Funct. Mater.* **2005**, *15*, 1617.
- 695 (17) Dante, M.; Garcia, A.; Nguyen, T.-Q. *J. Phys. Chem. C* **2009**, *113*, 1596.
- 696 (18) Liang, Y.; Feng, D.; Wu, Y.; Tsai, S.-T.; Li, G.; Ray, C.; Yu, L. *J. Am. Chem. Soc.* **2009**, *131*, 7792.
- 697 (19) Westerling, M.; Aarnio, H.; Österbacka, R.; Stubb, H.; King, S.; Monkman, A.; Andersson, M.; Jespersen, K.; Kesti, T.; Yartsev, A.; Sundström, V. *Phys. Rev. B* **2007**, *75*, 224306.
- 698 (20) Pacios, R.; Nelson, J.; Bradley, D. D. C.; Virgili, T.; Lanzani, G.; Brabec, C. *J. Phys.: Condens. Matter* **2004**, *16*, 8105.
- 699 (21) Clarke, T.; Ballantyne, A.; Jamieson, F.; Brabec, C.; Nelson, J.; Durrant, J. *Chem. Commun.* **2009**, *1*, 89.
- 700 (22) Peet, J.; Kim, J. Y.; Coates, N. E.; Ma, W. L.; Moses, D.; Heeger, A. J.; Bazan, G. C. *Nat. Mater.* **2007**, *6*, 497.
- 701 (23) Clarke, T. M.; Durrant, J. R. *Chem. Rev.* **2010**, *32*.
- 702 (24) Servaites, J. D.; Ratner, M. A.; Marks, T. *J. Appl. Phys. Lett.* **2009**, *95*, 163302.
- 703 (25) Servaites, J. D.; Yeganeh, S.; Marks, T. J.; Ratner, M. A. *Adv. Funct. Mater.* **2010**, *20*, 97.
- 704 (26) Son, H. J.; Wang, W.; Xu, T.; Liang, Y.; Wu, Y.; Li, G.; Yu, L. *J. Am. Chem. Soc.* **2011**, *133*, 1885.
- 705 (27) Hains, A.; Martinson, A. B. F.; Irwin, M. D.; Yan, H.; Marks, T. *Polym. Mater.* **2007**, *96*, 814.
- 706 (28) Lockard, J. V.; Wasielewski, M. R. *Phys. Chem. B Lett.* **2007**, *111*, 11638.
- 707 (29) Guo, J.; Ohkita, H.; Benten, H.; Ito, S. *J. Am. Chem. Soc.* **2009**, *131*, 16869.
- 708 (30) King, S. M.; Hintschich, S. I.; Dai, D.; Rothe, C.; Monkman, A. *P. J. Phys. Chem. C* **2007**, *111*, 18759.
- 709 (31) Carmichael, I.; Hug, G. *J. Phys. Chem. Ref. Data* **1986**, *15*, 1.
- 710 (32) Seki, H. *Faraday Trans.* **1992**, *88*, 35.
- 711 (33) Langan, J. R.; Salmon, G. A. *J. Chem. Soc., Faraday Trans. 1* **1982**, *78*, 3645.
- 712 (34) Yamamoto, Y.; Aoyama, T.; Hayashi, K. *J. Chem. Soc., Faraday Trans. 1* **1988**, *84*, 2209.
- 713 (35) Yamamoto, Y.; Nishida, S.; Ma, X.-H.; Hayashi, K. *J. Phys. Chem.* **1986**, *90*, 1921.
- 714 (36) Gersdorf, J.; Mattay, J.; Gorner, H. *J. Am. Chem. Soc.* **1987**, *109*, 1203.
- 715 (37) Garcia, A.; Brzezinski, J. Z.; Nguyen, T.-Q. *J. Phys. Chem. C* **2009**, *113*, 2950.
- 716 (38) King, S. M.; Hintschich, S. I.; Dai, D.; Rothe, C.; Monkman, A. *P. J. Phys. Chem. C* **2007**, *111*, 18759.
- 717 (39) Beljonne, D.; Shuai, Z.; Pourtois, G.; Bredas, J. L. *J. Phys. Chem. A* **2001**, *105*, 9.
- 718 (40) Sterpone, F.; Bedard-Hearn, M. J.; Rossky, P. J. *J. Phys. Chem. Lett.* **2009**, *113*, 3427.
- 719 (41) Bedard-Hearn, M. J.; Sterpone, F.; Rossky, P. J. *J. Phys. Chem. A* **2010**, *114*, 7661.
- 720 (42) Gelinas, S.; Pare-Labrosse, O.; Brosseau, C.-N.; Albert-Seifried, S.; McNeill, C. R.; Kirov, K. R.; Howard, I. A.; Leonelli, R.; Friend, R. H.; Silva, C. *J. Phys. Chem. C* **2011**, *115*, 7114.
- 721 (43) Hwang, I.; Moses, D.; Heeger, A. J. *Phys. Chem. C* **2008**, *112*, 4350.
- 722 (44) Pensack, R. D.; Banyas, K. M.; Barbour, L. W.; Hegadorn, M.; Asbury, J. B. *Phys. Chem. Chem. Phys.* **2009**, *11*, 2575.
- 723 (45) Howard, I. A.; Mauer, R.; Meister, M.; Laquai, F. *d. r. J. Am. Chem. Soc.* **2010**, *132*, 14866.
- 724 (46) Barbara, P. F.; Meyer, T. J.; Ratner, M. A. *J. Phys. Chem.* **1996**, *100*, 13148.
- 725 (47) Marcus, R. A.; Sutin, N. *Biochim. Biophys. Acta* **1985**, *811*, 265.
- 726 (48) Scharber, M. C.; Mühlbacher, D.; Koppe, M.; Denk, P.; Waldau, C.; Heeger, A.; Brabec, C. *Adv. Mater.* **2006**, *18*, 789.
- 727 (49) Ohkita, H.; Cook, S.; Astuti, Y.; Duffy, W.; Tierney, S.; Zhang, W.; Heeney, M.; McCulloch, I.; Nelson, J.; Bradley, D. D. C.; Durrant, J. *J. Am. Chem. Soc.* **2008**, *130*, 3030.

- 778 (50) Carsten, B.; Szarko, J. M.; Son, H.-J.; Wang, W.; Lu, L.; He, F.;  
779 Rolczynski, B. S.; Lou, S. J.; Chen, L. X.; Yu, L. *J. Am. Chem. Soc.* **2011**,  
780 133, 20468.  
781 (51) Beenken, W. J. D.; Pullerits, T. *J. Phys. Chem. B* **2004**, 108, 6164.  
782 (52) Risko, C.; Mcgehee, M. D.; Brédas, J.-L. *Chem. Sci.* **2011**, 2,  
783 1200.  
784 (53) Dias, F. B.; Pollock, S.; Hedley, G.; Palsson, L.-O.; Monkman,  
785 A.; Perepichka, I. I.; Perepichka, I. F.; Tavasli, M.; Bryce, M. R. *J. Phys.*  
786 *Chem. B* **2006**, 110, 19329.